Journal of the European Ceramic Society **18** (1998) 1045–1051

PII: S0955-2219(97)00206-9
0955-2219/98/$19.00 + 0.00

Oxidation Behavior of N-Containing Melilite Solid Solutions $Nd_2Si_{3-x}Al_xO_{3+x}N_{4-x}$

W. Chen, P. L. Wang* and D. S. Yan

The State Key Lab of High Performance Ceramics and Superfine Microstructure, Chinese Academy of Sciences, Shanghai 200050, People's Republic of China

(Received 28 July 1997; accepted 20 November 1997)

Abstract

Four compositions of N-containing Nd–melilite solid solution (Nd–M′) $Nd_2Si_{3-x}Al_xO_{3+x}N_{4-x}$ ($x=0, 0{\cdot}3, 0{\cdot}6, 1{\cdot}0$) prepared by hot-pressing technique were oxidized at 1000°C or 1250°C (only for $x=1{\cdot}0$) for 20 h in air in a TG unit. The phase compositions, densities, oxidation products, oxidation curves and microstructures of the samples were compared. The oxidation curves obtained indicate that the weight gains per unit area decrease obviously with increasing the Al substitution in Nd–M′, which is in good agreement with the corresponding changes in morphologies of the oxide-scale and cross-section of the samples, i.e. the cracks vary with the increase of Al content of Nd–M′, from large to small, and transit to pores. The oxidation mechanism of Nd–M′ was also discussed. © *1998 Published by Elsevier Science Limited. All rights reserved*

1 Introduction

In recent years, Si_3N_4-based ceramics with rare earth oxides (R_2O_3) as additives have attracted much attention. The importance of R_2O_3 for Si_3N_4 is recognized for several reasons. First, R_2O_3 can be accommodated into α-Si_3N_4 to form α-Sialon, thus providing the possibility to decrease the transient liquid phase content after sintering. Second, the R-Sialon glasses contain higher solubility of nitrogen than other Sialon glasses, thus the grain boundary glassy phases in Si_3N_4-based ceramics with R_2O_3 as sintering aids possess higher refractoriness. In the preparation procedure of rare-earth-stabilized Sialon ceramics, some rare-earth oxinitrides occur simultaneously as the crystalline intergranular phases in the material, among which N-containing melilite $R_2Si_3O_3N_4$ (abbreviated as R–M, R = Nd, Sm, Gd and Dy), is the most frequent one, especially in light rare-earth-oxide doped α-Sialon ceramics.[1] In the systems R–Si–Al–O–N (R = Nd, Sm), R–M is the only stable intergranular phase with high nitrogen contents.[2] Therefore, melilite becomes an important intergranular phase in R-α-Sialon or R-α-β-Sialon ceramics. However, the poor oxidation resistance of Y–M at 1000°C[3] with specific volume change of 30% after oxidation gives melilite a bad reputation to be used as a desirable intergranular phase in Sialon materials.

Recent work[4–7] indicates that aluminum can be dissolved in melilite, forming melilite solid solution $R_2Si_{3-x}Al_xO_{3+x}N_{4-x}$ (abbreviated as R–M′), which is expected to have an improved stability against oxygen because some of the Si–N are replaced by Al–O, and R–M′ is more easily formed for light rare earth elements. The solubility of Al in R–M′ decreases with the decrease in rare-earth ionic radii. Up to one Si can be replaced by Al for Nd–M′, whereas Y–M′ has the lowest observed Al solubility of about $x=0{\cdot}6$.[7] In order to understand the characteristic of the oxidation resistance of Sialon ceramics with R–M′ as the grain boundary phase, it is necessary to investigate the oxidation resistance of R–M′. This work intends to study the oxidation properties of Nd–M(M′) with the different Al contents, and to confirm that Nd–M′ do possess somewhat better oxidation resistance than Al-free melilite.

2 Experimental

The starting powders used were Si_3N_4 (UBE-10, Japan, 2·0 wt%O), AlN (Wuxi Chemical Plant, China, 1·3 wt%O), Nd_2O_3 (Yaolong Chemical

*To whom correspondence should be addressed.

Plant, China, 99·9%), Al_2O_3 (CR30, Wusong Chemical Plant, China, 99·5%). The surface oxygen in Si_3N_4 and AlN was taken into account by using formula of $Si_{2.94}N_{3.8}O_{0.175}$ and $Al_{1.023}NO_{0.034}$ in the compositional calculations. The composition used in this work was according to the formula of melilite solid solution $Nd_2Si_{3-x}Al_xO_{3+x}N_{4-x}$ with x = 0, 0·3, 0·6 and 1·0. The starting compositions after correction are listed in Table 1. The powders were mixed in absolute alcohol and milled in an agate mortar for 1·5 h. Pressed tablets of the mixed powders were fired at the temperature range of 1700–1780°C, which was depending on the Al contents of composition, by hot-pressing for 1 h in a graphite-resistance furnace in a flowing nitrogen atmosphere. The bulk densities of the samples were measured by the Archimedes principle. The samples with relative density (the ratio of measured density to theoretical one) greater than 99% were chosen for oxidation experiment.

The samples were cut into rectangular pieces with dimension of 12 mm×6 mm and 1 mm in thickness, and then were carefully polished on both surfaces. They were finally cleaned in boiling toluene and ultrasonically cleaned in acetone. The oxidation experiments were performed isothermally for 20 h at 1000°C and 1250°C (only for composition of x = 1·0) in a TG unit (LCT-2, Beijing Optical Plant, People's Republic of China. The software was modified by Shanghai Institute of Ceramics). The samples were exposed to air and were heated up to the temperature chosen with a rate of 20°C min^{-1}.

The surface and cross-section of the oxide scales were studied, respectively, with SEM KYKY 2000 and electron probe EPMA-8705QHII operating in back scattering mode, both equipped with an energy dispersive spectrometer (EDS). The crystalline phases present on the surface of samples after oxidation were identified with RAX-10 X-ray powder diffractometer. The cell parameters of Nd–M(M′) were obtained based on the X-ray (Cu Kα1, $\lambda = 1{\cdot}5405981$ Å) film data of Guinier-Hägg camera and used for the calculation of theoretical density of Nd–M(M′).

Table 1. Real compositions used in this work

Sample	*Nominal x value*	*Composition (wt%)*			
		Nd_2O_3	*Si_3N_4*	*AlN*	*Al_2O_3*
MN1	0	70·576	29.424		
MN2	0·3	70·551	26·678	1·874	0·898
MN3	0·6	70·507	23·699	2·632	3·162
MN4	1·0	70·454	19·734	3·663	6·149

3 Results and Discussion

3.1 Density and phase compositions

The samples were numbered with MNmn in this work, in which m equals to 1, 2, 3, 4 corresponding to Al contents of 0, 0·3, 0·6 and 1·0 respectively, *n* equals to 10 and 13, representing the oxidation temperatures of 1000°C and 1250°C respectively.

The relative density and phase present of sintered samples are listed in Table 2. In all samples, melilite was the major phase. In addition, there were $Nd_4Si_2O_7N_2$ (Nd–J phase), $Nd_{10}(SiO_4)_6N_2$ (Nd–H phase) and $NdSiO_2N$ (Nd–K phase) with very small amount separately appearing in Nd–M′ samples.

The phases present in the oxide scale of Nd–M(M′) are also listed in Table 2. $Nd_2Si_2O_7$ was the major product of oxidation. SiO_2, $NdAlO_3$, Nd–H, Nd–K and Nd–J phases with very small amounts were also found on the oxidized surface. There were small amounts of Nd–M′ left unoxidized in MN210, MN310 and MN413 samples, but a great number of unoxidized melilite appeared in MN110 and MN410, respectively.

From the formulas of Nd–M ($Nd_2Si_3O_3N_4$), Nd–K ($NdSiO_2N$), Nd-J ($Nd_4Si_2O_7N_2$), Nd–H [$Nd_{10}(SiO_4)_6N_2$] and $Nd_2Si_2O_7$, it can be found that these phases have a decreasing order in nitrogen contents. Therefore, the oxidation process of melilite could be deduced to be a gradual oxidation procedure. The whole oxidation reaction of MN110 can be described as follows:

$$Nd_2Si_3O_3N_4 + 3/2\ O_2 \rightarrow 2\ NdSiO_2N + SiO_2 + N_2\ (\uparrow)$$

$$Nd_2Si_3O_3N_4 + 9/4\ O_2 \rightarrow 1/2\ Nd_4Si_2O_7N_2 + 2\ SiO_2 + 3/2\ N_2\ (\uparrow)$$

Table 2. Density and phase present on the surface of $Nd_2Si_{3-x}Al_xO_{3+x}N_{4-x}$ before and after oxidation

No.	*x*	*Firing temperature (°C)*	*Relative density (%)*	*Phase present*[a]	*Oxidation temperature (°C)*	*Phase present on the oxidized surface*
MN110	0	1780	99·6	M(vs),K(vw)	1000	$Nd_2Si_2O_7$(s),M(s),SiO_2(w) H, J, K(tr)
MN210	0·3	1750	99·9	M′(vs),J(tr)	1000	$Nd_2Si_2O_7$(s),M′(w),SiO_2(w) $NdAlO_3$,H,J,K(tr)
MN310	0·6	1700	99·5	M′(vs),J,H(tr)	1000	$Nd_2Si_2O_7$(s),M′(w),SiO_2(w) $NdAlO_3$(vw),H,J,K(tr)
MN410	1·0	1700	99·9	M′(vs),J,H(tr)	1000	$Nd_2Si_2O_7$(s),M′(s),SiO_2(w) $NdAlO_3$(w),H,J,K(tr)
MN413	1·0	1700	99·9	M′(vs),J,H(tr)	1250	$Nd_2Si_2O_7$(s),M′(w),SiO_2(w) $NdAlO_3$(w)

[a] M, H, J, K: see text.

$$Nd_2Si_3O_3N_4 + 27/5\ O_2 \rightarrow 1/5\ Nd_{10}(SiO_4)_6N_2 + 9/5\ SiO_2 + 9/5\ N_2\ (\uparrow)$$

$$Nd_2Si_3O_3N_4 + 3\ O_2 \rightarrow Nd_2Si_2O_7 + SiO_2 + 2\ N_2\ (\uparrow)$$

The oxidation reactions of Nd–M′ are similar to Nd–M, in which $NdAlO_3$ was a oxidation product in addition to the ones mentioned above and amount of $NdAlO_3$ became larger with increasing in the Al substitution of composition (see more detailed discussion in next section).

3.2 Oxidation curves

The variation of the weight gains per unit area of samples with oxidation time is shown in Fig. 1(a). The weight gains of MN110 and MN410 are very small, the same as the base line drift of the TG apparatus (within 0·7 mg at 1000°C for 20 h). Compared to MN110 and MN410, the weight gains of MN210 and MN310 after oxidation in air at 1000°C for 20 h are greatly larger, in which the MN210's weight gain is higher than MN310's. As the weight gains of MN410 were within the drift of the base line when it oxidized at 1000°C for 20 h, the oxidation behavior of Nd–M′ ($x = 1·0$) at 1250°C for 20 h was carried out, whose weight gains were obviously larger than that at 1000°C (MN410).

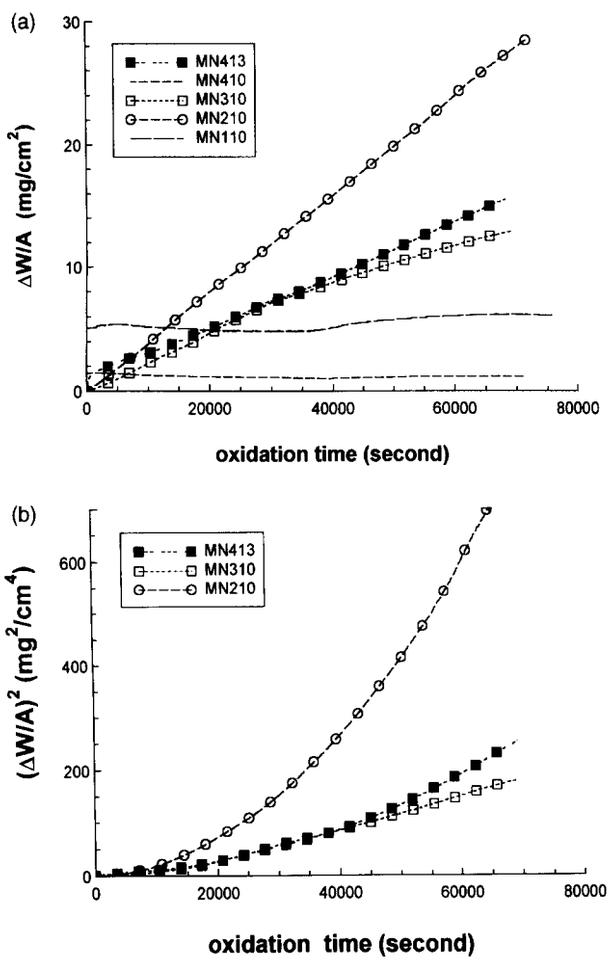

Fig. 1. Oxidation curves of Nd–M(M′). (a) weight gain curve, (b) squared weight gain curve. Note: in order to distinguish the curve of weight gains of MN110 versus oxidation time from the one of MN410 in Fig. 1(a), all weight gains of MN110 were moved to a higher level.

In Fig. 1(b), the squared weight gains of MN210, MN310 and MN413 all have concave shape, fairly different from the linear shape of a diffusion controlled oxidation procedure with constant diffusion area, or the convex shape of a procedure with decreasing in diffusion area.

3.3 Microstructure of the samples

The microstructures of samples, before and after oxidation at 1000°C or 1250°C for 20 h, are shown in Figs 2–4 in which Fig. 2(a) and (b) are SEM photos of samples MN110 and MN310 before oxidation. Figures 3 and 4, respectively, show the surface and cross-section of oxide scale of MN110, MN210, MN310, MN410 and MN413.

It can be seen from the micrograph of matrix (without oxidation) of MN110 that melilite phase (grey) with very small amount of pores (black) is the major characteristic and the other phase is neglectable [some uncleaned polish diamond grains are also shown on the surface of matrix of MN110 and MN310, cross-section of MN110 and MN210 in Fig. 2(a) and (b), and Fig. 4(a) and (b), respectively]. When compositions of Nd–M′ were towards the increase of Al substitution, the microstructures of the samples showed the increase in amount of grain boundary phase. As seen from Fig. 2(b), the white colour in the micrograph, which is taken on the surface of matrix of composition Nd–M′ ($x = 0·6$), is corresponding to the grain boundary Nd–J and Nd–H phases. It is interesting to note the differences that exist in the oxide surfaces, i.e. there are a few tiny cracks on the surface of oxide scale of MN110, a lot of large cracks appear on the one of MN210 and a few cracks and pores exist in MN310, as shown in Fig. 3. The oxide scale of MN410 has the characteristic of a few pores, and MN413, a large amount of pores. It can be concluded from the micrographs of the oxide scale and cross-section of the samples that the cracks vary with the increase of Al content of M′, from large to small, and transit to pores.

3.4 Oxidation mechanism of Nd–M′

The following items can be obtained from the above results: (1) the oxidation weight gain is related to the Al content of Nd–M′, in general, decreasing with the increase of Al content. (2) the oxidation weight gain of Nd–M(M′) increases with the increase of oxidation temperature. (3) the effect of intergranular glass of the sample on oxidation

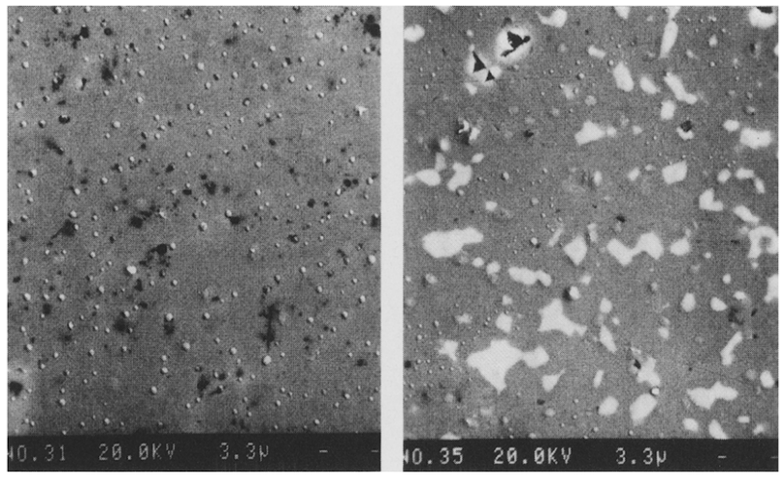

Fig. 2. SEM micrographs of (a) Nd–M (x = 0) and (b) Nd–M′ (x = 0·6) before oxidation.

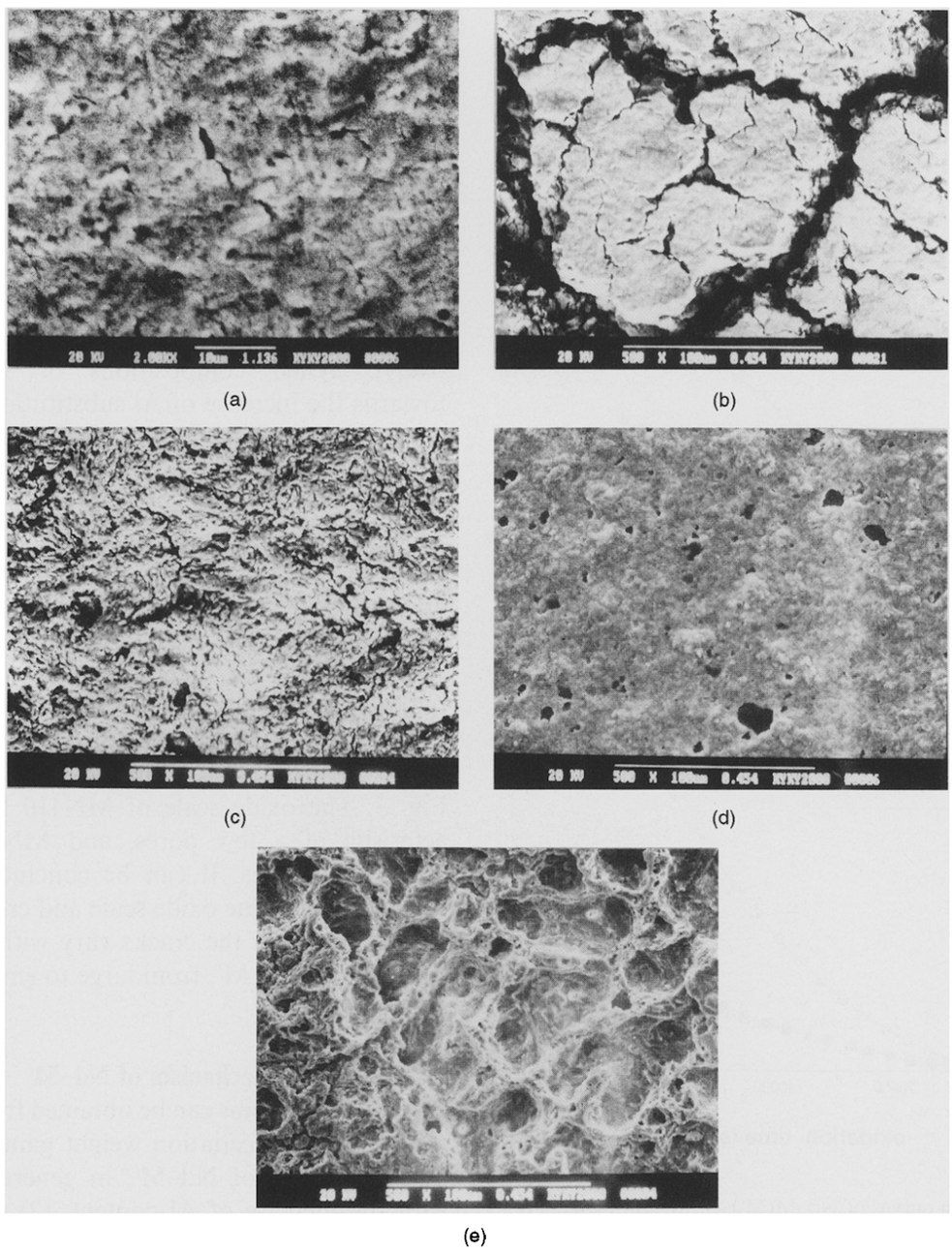

Fig. 3. SEM micrographs of the oxidized surfaces of Nd–M(M′). (a) x = 0, (b) x = 0·3, (c) x = 0·6, (d) x = 1·0, (e) x = 1·0. Oxidation temperatures of samples (a)–(d) and (e) are 1000°C and 1250°C for 20 h, respectively.

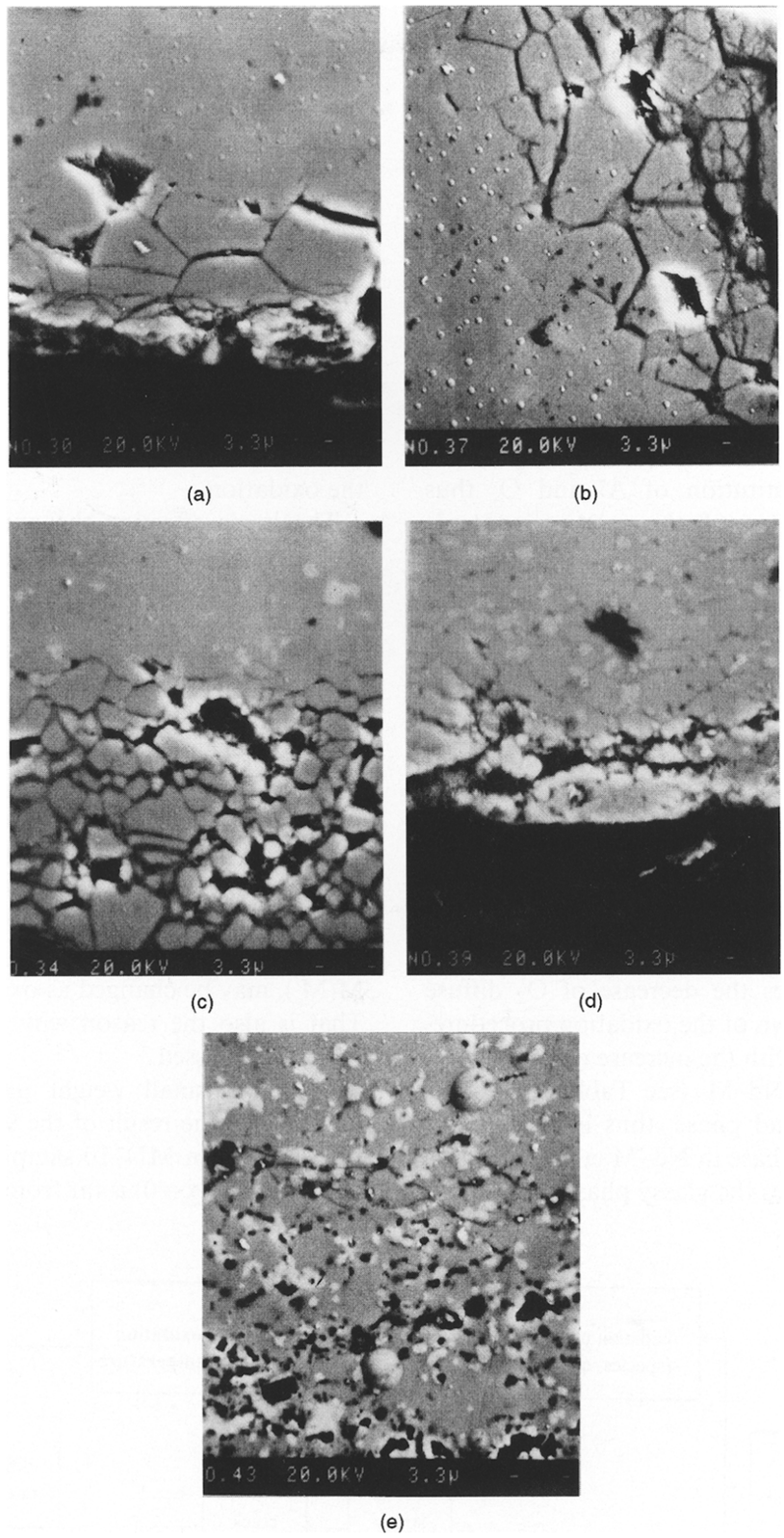

Fig. 4. SEM micrographs of the cross-section of oxide scale of Nd–M(M′). (a) x = 0, (b) x = 0·3, (c) x = 0·6, (d) x = 1·0, e) x = 1·0. Oxidation temperatures of samples (a)–(d) and (e) are 1000°C and 1250°C for 20 h, respectively.

cannot be neglected. This is shown by the small oxidation level of MN110 and will be discussed in detail later.

It is considered that the oxidation reaction first takes place in the intergranular phase of the material, and then in the grain because of the high energy state of intergranular phase.

It is reported that the oxidation product of Si_3N_4 is chiefly glassy phase, and for Sialon, the glassy products are partly devitrified because of additive ion.[8,9] In Nd–M(M′) the Nd ion content is very high, the oxidation products are mostly devitrified to form $Nd_2Si_2O_7$, SiO_2 and $NdAlO_3$ crystalline phases. $Nd_2Si_2O_7$ and SiO_2 crystalline phases have

a large specific volume. Their formation and the effusion of N_2 during oxidation can induce stress in the material, which results in the formation of cracks, thus increasing in the O_2 diffusion area and speeding up the oxidation procedure. In the oxidation reaction sequence of Nd–M, $Nd_2Si_3O_3N_4 + 3\ O_2 \rightarrow Nd_2Si_2O_7 + SiO_2 + 2N_2$, the relative specific volume change can be calculated by $\Delta V/V = (V_{SiO_2} + V_{Nd_2Si_2O_7} - V_M)/V_M$, supposing that the products (solid) are all crystalline phases. The $\Delta V/V$ of Nd–M is 21·2%. Although it is smaller than that of Y–M (30%), it is big enough to induce stress and cracks in Nd–M sample.

For Nd–M′, the oxidation products are increased because of the substitution of Al and O, thus results in the changes of the relative contents and the volumes of the products. The oxidation reaction sequence of Nd–M′ is described as: $Nd_2Si_{3-x}Al_xO_{3+x}N_{4-x} + (3-3x/4)\ O_2 \rightarrow (1-x/2)\ Nd_2Si_2O_7 + x\ NdAlO_3 + SiO_2 + (2-x/2)N_2$. The relative specific volume change of Nd–M′ by oxidation, $(V_{SiO_2} + (1\text{-}x/2)V_{Nd_2Si_2O_7} + xV_{NdAlO_3} - V_{M'})/V_{M'}$, decreases with the increase of Al content x in composition, and reaches its value of 8·4% at the Al content x = 1·0. At the same time, the amount of N_2, which is one of oxidation products of Nd–M′, decreases with the increase of x value of composition, accordingly, which lessens the stress and cracks of samples. The lessening of cracks in oxidized samples implies the decrease of O_2 diffuse area and slowing down of the oxidation procedure. On the other hand, with the increase of Al content, the composition of Nd–M′ (see Table 1) approaches that of the liquid phase, thus increasing the extent of the glassy phase in Nd–M′ after sintering. Furthermore, it makes the glassy phase of material rich in oxygen, which can lower the glass softening temperature of glassy phase. Therefore, the increase of Al content in Nd–M′ can relieve stress and lessen cracks during oxidation, thus decreasing the O_2 diffusion area and alleviating oxidation of the samples. It is obvious that the increase of the amount of glassy phase in the samples means the increase of O_2 diffusion paths and diffusion area, which will result in quickening of oxidation. The rise of the oxidation temperature obviously speeds up the diffusion of O_2 and quickens the oxidation procedure. But at higher temperature, the glassy phase in the samples can be softened, therefore stress can be relieved more easily, thus alleviating the oxidation.

The items affecting the oxidation procedure of Nd–M(M′) and their relationships are illustrated in Fig. 5, which shows the comprehensive consideration of above analysis. The oxidation procedure of Nd–M(M′) is affected by the above-mentioned factors. Under different situations, factors play a different role, major or minor. The effect of the extent of glassy phase of Nd–M(M′) samples on O_2 diffusion path and area is quickly induced at the beginning of oxidation. However, the effect of cracks, which are introduced by volume expansion during oxidation, on diffuse area and stress is a slow and long process. So the status of factors which affect the oxidation procedure of Nd–M(M′), may be changed as oxidation time goes on. That is also the reason why the oxidation curves might get crossed.

The very small weight gains of MN110 are regarded as the result of the very small amount of glassy phase in MN110 sample since the composition of MN1 (x = 0) is far from that of liquid phase.

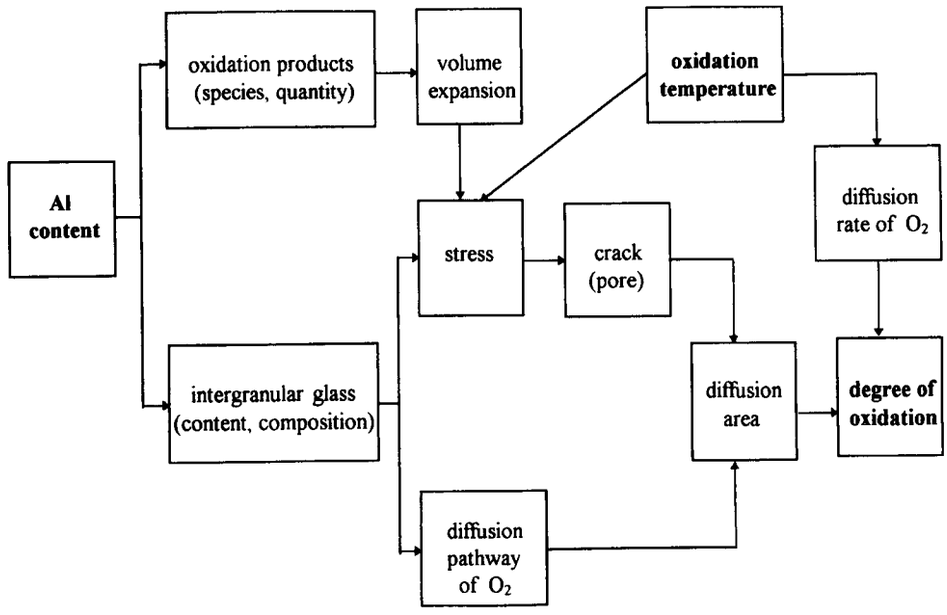

Fig. 5. Scheme of items affecting the oxidation procedure of Nd–M(M′).

although the oxidation weight gains of MN110 and MN410 are at the same low level, but the reasons for this are distinct. The former is because of the small amount of glassy phase in the initial sample, which leads to the smaller O_2 diffusion path and amount of oxidation products, thus resulting in a small volume expansion and tiny cracks from which nitrogen can effuse during oxidation. Whereas the latter (MN410) is because of the small volume expansion led by the big Al content in its composition, although its oxidation product amount is not small. In its oxidation, pores exist from which N_2 effuses. From the comparison of oxidation behavior of MN110 and MN410, it is understandable that the latter is functionally superior to the former in oxidation resistance.

4 Conclusion

- The oxidation weight gain per unit area of Nd–M′ is related to the Al contents of compositions, decreasing with the increase of Al substitution, which is in good agreement with the corresponding changes in morphologies of the oxide-scale and cross-section of Nd–M′, i.e. the cracks of the samples after oxidation vary with the increase of Al content of Nd–M′, from large to small, and transit to pores. Whereas the oxidation weight gain of Nd–M′ increases with the increase of oxidation temperature.
- There are several factors to affect the oxidation behavior of Nd–M(M′). Because of the substitution of Al and O, the oxidation products of Nd–M(M′) are changed during oxidation and the relative specific volume decreases with the increase of Al content of the compositions and reaches its value of 8·4% at the Al content $x = 1{\cdot}0$, thus resulting in lessening the stress and cracks and slowing down the oxidation procedure. On the other hand, the effect of the content and composition of intergranular glassy phase of Nd–M(M′) on oxidation cannot be neglected.

Acknowledgement

The authors acknowledge financial support from the National Natural Science Foundation of the People's Republic of China. (No.59572009).

References

1. Wang, P. L., Sun, W. Y. and Yen, T. S., Sintering and formation behaviour of R-α-Sialons (R = Nd, Sm, Gd, Dy, Er and Yb). *Eur. J. Solid State Inorg. Chem*, 1994, **31**(2), 93.
2. Sun, W. Y., Yan, D. S., Gao, L., Mandal, H. and Thompson, D. P., Subsolidus phase relationships in the systems Ln_2O_3–Si_3N_4–AlN–Al_2O_3 (Ln = Nd, Sm). *J. Eur. Ceram. Soc*, 1995, **15**(4), 349.
3. Patel, J. K. and Thompson, D. P., The low-temperature oxidation problem in yttria-densified silicon nitride ceramics. *Br. Ceram. Trans*, 1988, **87**, 70.
4. Slasor, S., Liddell, K. and Thompson, D. P., The role of Nd_2O_3 as an additive in the formation of α and β Sialons. *Br. Ceram. Proc*, 1986, **37**, 51–64.
5. Käll, P.-O. and Ekström, T., Sialon ceramics made with mixtures of Y_2O_3-Nd_2O_3 as sintering aids. *J. Eur. Ceram. Soc*, 1990, **6**, 119–127.
6. Cheng, Y. B. and Thompson, D. P., Aluminium-containing nitrogen melilite phases. *J. Am. Ceram. Soc*, 1994, **77**, 143–148.
7. Wang, P. L., Tu, H. Y., Sun, W. Y., Yan, D. S., Nygren, M. and Ekström, T., Study on the solid solubility of Al in the melilite systems $R_2Si_{3-x}Al_xO_{3+x}N_{4-x}$ with R = Nd, Sm, Gd, Dy and Y. *J. Eur. Ceram. Soc*, 1995, **15**, 689–695.
8. Persson, J., Käll, P.-O. and Nygren, M., Interpretation of the parabolic and nonparabolic oxidation behavior of silicon oxinitride. *J. Am. Ceram. Soc*, 1994, **75**, 3377.
9. Persson, J., Käll, P.-O. and Nygren, M., Parabolic-nonparabolic oxidation kinetics of Si_3N_4. *J. Eur. Ceram. Soc*, 1993, **15**, 177.